

# Transbilayer coupling of obstructed lipid diffusion in polymer-tethered phospholipid bilayers†

Miranda A. Deverall,<sup>a</sup> Sumit Garg,<sup>a</sup> Karin Lüttke,<sup>b</sup> Rainer Jordan,<sup>b</sup> Jürgen Rühle<sup>c</sup> and Christoph A. Naumann<sup>\*\*</sup>

Received 17th January 2008, Accepted 28th May 2008

First published as an Advance Article on the web 15th July 2008

DOI: 10.1039/b800801a

The current study reports on the inter-leaflet coupling of obstructed lipid diffusion in a polymer-tethered phospholipid bilayer, where the obstruction of diffusion is caused by lipopolymers which form non-bilayer-spanning membrane pinning sites in the bottom leaflet of the bilayer. Monolayer-specific wide-field single molecule fluorescence microscopy experiments of fluorescence-tagged phospholipids (TRITC-DHPE) over a wide range of lipopolymer concentrations,  $c_{\text{tether}}$ , reveal a strong, polymer-induced inter-leaflet coupling of obstructed lipid diffusion for different types of lipopolymers, including those based on poly(ethylene glycol), poly(2-methyl-2-oxazoline), and poly(2-ethyl-2-oxazoline) as the hydrophilic polymer moiety. Remarkably, the degree of inter-leaflet diffusional coupling can be regulated by the cholesterol (CHOL) content which affects membrane bending elasticity. This latter finding suggests that the inter-leaflet coupling of obstructed diffusion is caused by polymer-induced bilayer deformations around membrane pinning sites, thus creating membrane-spanning regions of high membrane tension. Because the inter-leaflet coupling of obstructed diffusion at an elevated CHOL molar concentration also decreases with increasing  $c_{\text{tether}}$ , we hypothesize that both leaflets of the bilayer are morphologically decoupled at high  $c_{\text{tether}}$  with the outer (lipopolymer-free) monolayer being flatter than the inner one. Our findings could be of biological relevance because a similar mechanism of transbilayer coupling of obstructed diffusion may occur in some regions of cellular membranes.

## Introduction

One of the tenets of modern cell biology and membrane biophysics is that a plasma membrane represents a highly complex compartmentalized system showing a great diversity of dynamic processes. Membrane compartmentalization and the resulting length-scale-dependent membrane diffusion processes are caused largely by the underlying cytoskeleton and, to a lesser extent, by the extracellular matrix (ECM), either due to direct interactions or *via* diffusion obstacles of membrane constituents linked to both filamentous environments.<sup>1,2</sup> Surprisingly, phospholipids also show length-scale-dependent diffusion properties on cell surfaces.<sup>3,4</sup> One obvious mechanism is that the interaction is transmitted across the membrane by transmembrane proteins acting as *membrane-spanning* pickets, as proposed in the picket-fence model.<sup>3,4</sup> Such a model does not consider, however, the case of *non-bilayer-spanning* pickets such as cytoskeleton-binding lipids. It is known that filamentous proteins of the cytoskeleton, including spectrin and filamin, also possess lipid binding domains.<sup>5,6</sup> Furthermore, there is growing evidence that phosphorylated derivatives of phosphatidylinositol such as

phosphatidylinositol 4,5-bisphosphate (PIP<sub>2</sub>) play a critical role by regulating the actin cytoskeleton *via* the modulation of activity and targeting of actin regulatory proteins, and that these lipids may create membrane–cytoskeleton attachments by electrostatically binding to particular cytoskeleton-binding proteins such as MARCKS.<sup>7,8</sup> This observation gives rise to the central question behind the current study: *how can non-bilayer-spanning diffusion obstacles, e. g., lipids linked to cytoskeleton-binding proteins, affect the lateral diffusion of non-bilayer-spanning molecules in the opposite leaflet of the bilayer?* Here we present experimental evidence for one possible mechanism of coupling of obstructed diffusion in the presence of non-bilayer-spanning diffusion obstacles using a model membrane platform based on polymer-tethered membranes.

The polymer-tethered phospholipid bilayer, which represents a specific type of polymer-supported membrane, is characterized by an adjustable concentration of lipopolymers (polymer-tethered lipids),  $c_{\text{tether}}$ , in one of its monolayers.<sup>9–11</sup> This model membrane system is well-suited to the incorporation and study of transmembrane proteins in a planar membrane geometry under non-denaturing conditions because the bilayer–substrate distance can be increased sufficiently using a hydrophilic polymer layer as a spacer.<sup>9,11,12–16</sup> For example, some of us reported that integrin-mediated adhesion to ligand-functionalized vesicles is enhanced 30 fold if these receptors are incorporated into a polymer-tethered bilayer *versus* a solid-supported bilayer (without polymer layer).<sup>15</sup> Recently, it also has been reported that polymer-tethered membranes are well-suited to controlling the frictional coupling between membrane proteins and a solid substrate because the thickness and the density of the polymer

<sup>a</sup>Department of Chemistry and Chemical Biology, Indiana University-Purdue University Indianapolis, Indianapolis, IN 46202-3274. E-mail: naumann@chem.iupui.edu

<sup>b</sup>Wacker-Lehrstuhl für Makromolekulare Chemie, Department Chemie, Technische Universität München, 85747 Garching, Germany

<sup>c</sup>Department of Microsystem Engineering, Universität Freiburg, 79110 Freiburg, Germany

† Electronic supplementary information (ESI) available: Coupling of obstructed TRITC-DHPE diffusion in polymer-tethered phospholipid bilayers. See DOI: 10.1039/b800801a

layer can be adjusted.<sup>17</sup> Existing reports on lipid diffusion properties in these membranes are conflicting.<sup>10,11,13,18</sup> Some of us recently showed that physisorbed poly(2-ethyl-2-oxazoline) lipopolymers of a degree of polymerization of  $n = 85$  may profoundly obstruct the lateral diffusion of transmembrane proteins (bacteriorhodopsin) and lipids in polymer-tethered membranes.<sup>13</sup> Obstruction of lipid diffusion was also reported for polymer-tethered membranes on benzophenone-modified substrates.<sup>10,18</sup> In both of these cases, it has been reported that there is a coupling of obstructed diffusion between both leaflets of the bilayer. In contrast, systematic fluorescence recovery after photobleaching (FRAP) experiments on membrane systems with silane-modified poly(2-methyl-2-oxazoline) did not show any notable obstruction of the bilayer fluidity over a significant tethering (lipopolymer) concentration range of  $c_{\text{tether}} = 0$ –20 mol% and provided no indication for a coupling of obstructed diffusion.<sup>11</sup> The conflicting diffusion data reported suggest that the lipopolymer-induced obstruction of lipid diffusion may depend on multiple factors, including the chemical nature of the polymer, the viscosity and thickness of the polymer layer, and the type of linkage between polymer chains and solid substrate. Interestingly, strong inter-leaflet coupling of obstructed lipid diffusion was also observed on solid-supported phospholipid bilayers after adsorption of polymers to the top leaflet of the bilayer.<sup>19</sup> In that case, obstructed lipid diffusion underneath adsorbed polymers has been interpreted using a model of slaved diffusion.<sup>20</sup> Existing data regarding inter-leaflet diffusional coupling in phospholipid bilayers without lipopolymers ( $c_{\text{tether}} = 0$ ) are also contradictory. For example, FRAP and fluorescence correlation spectroscopy (FCS) studies in such bilayer systems showed no notable leaflet-specific differences in lipid diffusion.<sup>21,22</sup> In contrast, NMR studies on lipid bilayers on silica beads revealed pronounced differences between distal and proximal monolayers of the bilayer, thus suggesting a weaker inter-leaflet coupling of lipid diffusion.<sup>23</sup> The reason for these contradictory results remains unknown, but could be related to differences in substrates or sample preparations. Interestingly, MD simulations in a pure lipid bilayer showed a notably weaker distance-dependent displacement correlation between two lipids in opposing leaflets relative to lipids in the same leaflet $\ddagger$ . Such a weaker coupling seems to be counterintuitive if one considers the partial overlap and entanglement of lipid acyl chains between both leaflets. However, NMR relaxation and MD simulations have shown that lipid lateral diffusion is primarily modulated by hydrogen bonding and electrostatic interactions at the bilayer–water interface, and is less influenced by the boundary region between both lipid monolayers.<sup>24</sup> In fact, the relatively weak influence on lipid diffusion due to chain overlap/entanglement in the central region of the bilayer appears reasonable in light of two experimental observations: (i) the segmental order parameter of acyl chains in the central membrane region is particularly small,<sup>25</sup> and (ii) lipid lateral diffusion does not depend on the degree of acyl chain interdigitation.<sup>26</sup>

In the current wide-field single molecule fluorescence imaging study, we show that the lateral diffusion of phospholipids in a polymer-tethered phospholipid (1-stearoyl-2-oleoyl-*sn*-glycero-

3-phosphocholine, SOPC) bilayer containing either poly(2-ethyl-2-oxazoline) or poly(2-methyl-2-oxazoline) lipopolymers is also obstructed in the opposite leaflet of the bilayer, which is free of lipopolymers. Intriguingly, the degree of coupling of obstructed diffusion between both leaflets depends on bilayer bending elasticity and  $c_{\text{tether}}$ . The data are obtained by analyzing the lateral diffusion of the fluorescently labeled lipid molecules *N*-(6-tetramethylrhodaminethiocarbamoyl)-1,2-dihexadecanoyl-*sn*-glycero-3-phosphoethanolamine, triethylammonium salt (TRITC-DHPE) for each monolayer separately and by correlating the two data sets. To understand this phenomenon better, in addition the bending elasticity is varied by adding different amounts of cholesterol (CHOL) to the SOPC bilayer. Our current findings are discussed in terms of polymer-induced bilayer deformations around tethering points, which create regions of high membrane tension. It is hypothesized that a similar mechanism of transbilayer coupling of obstructed diffusion may occur in plasma membranes.

## Results and discussion

The data in Fig. 1, which caught our curiosity and largely motivated this study, show representative square-displacement,  $r^2$ , histograms of outer and inner monolayer tracking experiments of the dye-labeled lipid TRITC-DHPE in a polymer-tethered phospholipid bilayer over a wide range of  $c_{\text{tether}} = 2, 10, 20,$  and  $30$  mol% (composition of the inner monolayer: phospholipid (SOPC) and lipopolymer {dioctadecylamine [poly(2-ethyl-2-oxazoline) 8988] (DODA-E<sub>85</sub>)}; composition of the outer monolayer: SOPC). The number of monomers per polymer,  $n$ , of DODA-E<sub>85</sub> is  $n = 85$ . As recently reported, the diffusion data of TRITC-DHPE in the inner (lipopolymer-containing) monolayer in Fig. 1 are well-described by existing models of obstacle-induced obstructed diffusion.<sup>13</sup> Remarkably, Fig. 1 also shows that the histograms representing tracer diffusion in the opposite (lipopolymer-free) monolayer are comparable at each  $c_{\text{tether}}$  studied, thus indicating a surprisingly strong coupling of obstructed diffusion between both leaflets of the bilayer. This strong inter-leaflet coupling phenomenon is also supported by Fig. 2, where the tracking data are illustrated in the form of  $\langle r^2 \rangle - c_{\text{tether}}$  (Fig. 2, left) and  $IF - c_{\text{tether}}$  plots (Fig. 2, right). Here  $\langle r^2 \rangle$  is the mean square displacement and  $IF$  is the immobile fraction. Fig. 2 (left) shows that the inner and outer leaflets are characterized by comparable  $\langle r^2 \rangle$  for each  $c_{\text{tether}}$  studied. In both cases, the linear decrease of  $\langle r^2 \rangle$  with increasing  $c_{\text{tether}}$  and the blocking of lateral lipid diffusion at  $c_{\text{tether}} \approx 40$  mol% can be observed. As shown in Fig. 2 (right),  $IF$  is almost identical between both leaflets of the bilayer if plotted as a function of  $c_{\text{tether}}$ . The asymptotic behavior of both  $IF - c_{\text{tether}}$  plots indicates a percolation-like behavior with the percolation threshold at  $\sim 40$  mol%.<sup>13</sup> The strong inter-leaflet coupling of obstructed lipid diffusion observed in Fig. 1 and 2 is quite remarkable. In the following, we will explore this intriguing phenomenon in more detail.

Lipid flip flop and/or transbilayer diffusion of lipids at holes/edges of the bilayer might represent a potential artifact that could explain the data in Fig. 1 and 2. In fact, Crane and Tamm have reported significant flip flop of labeled lipids using similar membrane systems.<sup>27</sup> On the other hand, we have recently shown that a considerable asymmetry in the lipid composition of

$\ddagger$  S. Feller, personal communication.

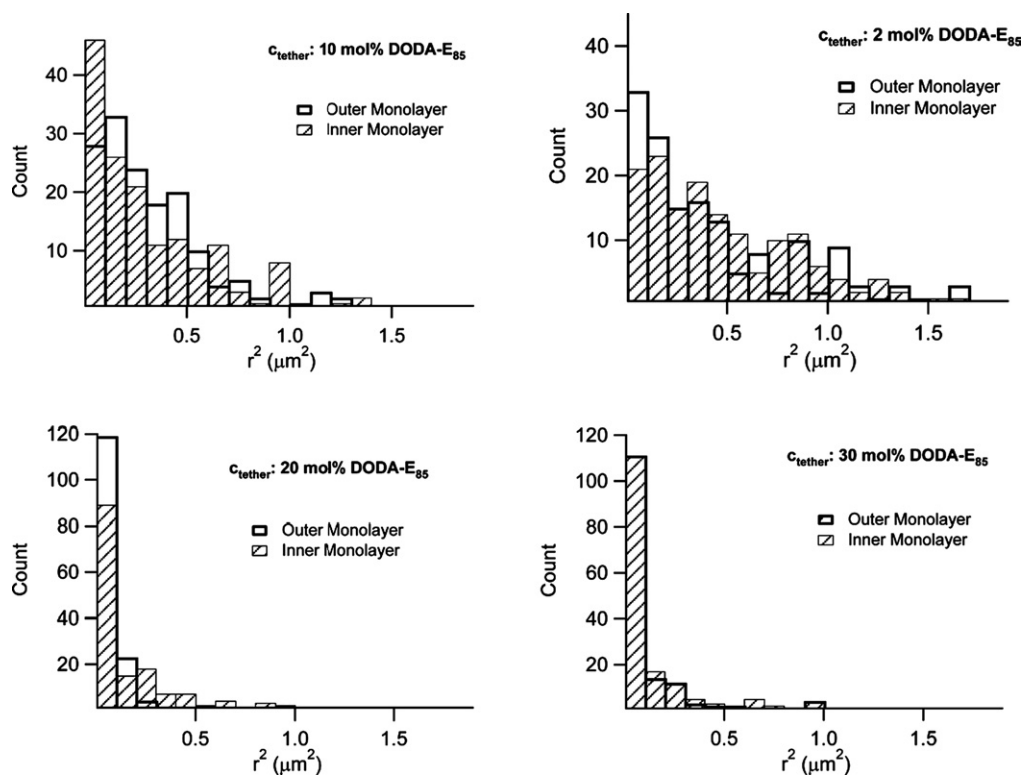


**Fig. 1** Representative square-displacement  $r^2$  histograms comparing TRITC-DHPE lateral mobility in both monolayers of a polymer-tethered phospholipid bilayer at tethering concentrations of  $c_{\text{tether}} = 2, 10, 20,$  and  $30$  mol%.

polymer-tethered membranes can be maintained after bilayer formation using Langmuir–Blodgett and Schaefer transfers.<sup>28</sup> To rule out an experimental artifact based on lipid flip flop and/or transbilayer diffusion, two sets of control experiments were performed in which the fluorescently labeled lipopolymers 1,2-dipalmitoyl-*sn*-glycero-3-phosphatidylethanolamine-*N*-[amino (polyethylene glycol)2000]-TAMRA (DPPE-PEG2000-TAMRA) were incorporated either into the inner or outer monolayers of the polymer-tethered bilayer and the tracking data were

compared to those obtained using TRITC-DHPE. The rationale behind this approach is that the flipping of lipopolymer tracers with their bulky hydrophilic polymer moiety across the hydrophobic acyl chain region of the bilayer should be energetically less favorable than flip flop processes of TRITC-labeled phospholipids. In addition, one should expect that the lateral mobility of lipopolymers in the inner monolayer is suppressed significantly due to polymer–polymer and polymer–substrate interactions if compared to the lateral mobility of the same tracers in the

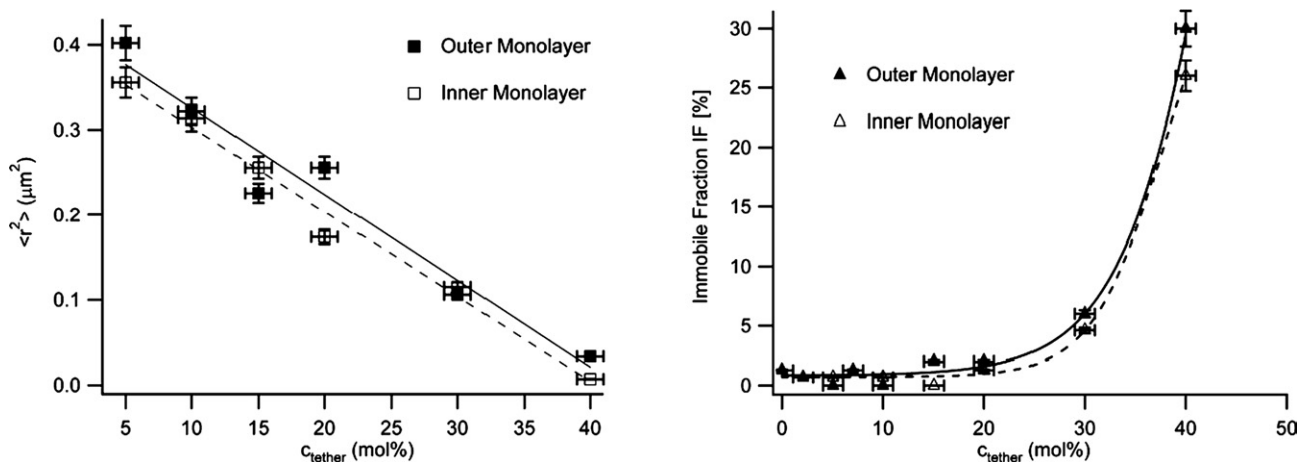


**Fig. 2** Mean square displacement  $\langle r^2 \rangle$  (left) and immobile fraction  $IF$  (right) from separate TRITC-DHPE tracking experiments in the inner and outer monolayers of the polymer-tethered bilayer based on DODA-E<sub>85</sub> plotted vs.  $c_{\text{tether}}$ . Both graphs illustrate a strong coupling of obstructed diffusion. The solid and dashed lines in the  $\langle r^2 \rangle$ - $c_{\text{tether}}$  plots represent the best linear fits of outer and inner monolayer data, respectively. Corresponding lines in  $IF$ - $c_{\text{tether}}$  plots are included to guide the eye.

**Table 1** Summarized  $\langle r^2 \rangle$  results obtained from tracking experiments of lipid (TRITC-DHPE) and lipopolymer (TRITC-DSPE-PEG2000) tracer molecules in the inner and outer leaflets of a polymer-tethered phospholipid bilayer for varying concentrations of polymer-tethered lipids DODA-E<sub>85</sub>,  $c_{\text{tether}}$ . The  $\langle r^2 \rangle$  data are characterized by an error margin of  $\Delta\langle r^2 \rangle = \pm 5\%$

$c_{\text{tether}}/\text{mol}\%$	$\langle r^2 \rangle$ lipid (inner)/ $\mu\text{m}^2$	$\langle r^2 \rangle$ lipid (outer)/ $\mu\text{m}^2$	$\langle r^2 \rangle$ lipopolymer (inner)/ $\mu\text{m}^2$	$\langle r^2 \rangle$ lipopolymer (outer)/ $\mu\text{m}^2$
5	0.36	0.40	0.007	0.34
10	0.31	0.32	0.004	0.30
15	0.26	0.23		0.29
20	0.17	0.26		0.21
30	0.12	0.11		0.13
40	0.01	0.03		0.03

outer monolayer. At the same time, DPPE-PEG2000-TAMRA is an excellent probe to mimic lipid lateral diffusion because the lipid anchor is not expected to penetrate notably into the opposite leaflet<sup>29</sup> and because the bulky hydrophilic polymer moiety does not significantly contribute to the lateral diffusion of these probes (*i.e.*, lipid/lipopolymer diffusion is determined by the interior of the bilayer where viscosity is much higher than water). Table 1 summarizes  $\langle r^2 \rangle$  values for different  $c_{\text{tether}}$  obtained from tracking experiments using TRITC-DHPE and DPPE-PEG2000-TAMRA tracers in either the outer or inner monolayers of this asymmetric bilayer system. The data in Table 1 reveals that the lateral mobility of lipopolymer and phospholipid tracers in the outer monolayer is almost identical at each  $c_{\text{tether}}$  studied, thus verifying that the coupling of obstructed diffusion is not caused by the flip flop- and/or transbilayer diffusion-induced formation of a symmetric TRITC-DHPE distribution in the bilayer. Table 1 also does not support the concept of flip flop/transbilayer diffusion of tethered lipids because  $\langle r^2 \rangle$  from tracking experiments on DPPE-PEG2000-TAMRA in the inner leaflet at low  $c_{\text{tether}}$  is almost 2 orders of magnitude smaller than corresponding experiments using the same tracer molecules in the outer leaflet. Furthermore, a statistical analysis of  $r^2$  values from individual tracks at  $c_{\text{tether}} = 5$  mol% shows that there is only  $\sim 3\%$  overlap if one compares lipopolymer tracers in both leaflets (data not shown). Overall, the two control experiments using DPPE-PEG2000-TAMRA provide direct experimental evidence that the observed coupling phenomenon of obstructed diffusion is *not caused* by flip flop and/or transbilayer diffusion of tracer molecules and tethered lipids. We should emphasize that these control experiments do not imply that there is no flip flop of lipids.

As reported before, the analysis of the tracking data in terms of cumulative distribution functions (CDFs) provides a useful tool to obtain additional information about the type of diffusion $\S$ . Previously, we reported that the TRITC-DHPE and bacteriorhodopsin tracking data obtained at low  $c_{\text{tether}}$  are well-described by the theoretical CDF for Brownian diffusion (eqn 2) but that the anomalous diffusion model (eqn 3) should be applied at higher  $c_{\text{tether}}$ .<sup>13</sup> There, the observed deviations from Brownian

diffusion at high  $c_{\text{tether}}$  were interpreted in terms of a moderate clustering among lipid anchors of lipopolymers, thus creating a more heterogeneous distribution of diffusion obstacles. To evaluate whether such changes in the lateral distribution of tethered lipids in the inner monolayer can be “detected” by tracer molecules in the outer monolayer, CDF analysis was conducted on tracking data obtained from both the inner and outer leaflets of the bilayer. Fig. 3 (left) illustrates representative experimental CDFs (data points) of the DODA-E<sub>85</sub> system and the corresponding fitting curves using the theoretical CDF for Brownian (dashed) and anomalous diffusion (solid) at  $c_{\text{tether}} = 10$  and 30 mol%. Fig. 3 (left) shows for both monolayers that experimental and theoretical CDFs of Brownian diffusion match well at  $c_{\text{tether}} = 10$  mol%, supporting the concept of a homogeneous distribution of diffusion obstacles in both monolayers. In contrast, at  $c_{\text{tether}} = 30$  mol%, both monolayers are better described by the anomalous diffusion model, thus suggesting a heterogeneous distribution of diffusion obstacles in both monolayers. As illustrated in Fig. 3 (right), a comparable result can be obtained by analyzing the monolayer-specific  $\chi^2$ - $c_{\text{tether}}$  plots obtained from the fitting results of the experimental CDFs using the theoretical CDF of Brownian diffusion (eqn 2). Here tracking data from the inner and outer leaflets show small values of  $\chi^2$  at low  $c_{\text{tether}}$  indicating Brownian diffusion and increased  $\chi^2$  indicating anomalous diffusion at higher  $c_{\text{tether}}$ . Overall, the data in Fig. 3 reveal that diffusion obstacles in the outer (lipopolymer-free) monolayer represent a mirror image of the obstacle distribution in the inner one.

Next, we explored the strength of inter-leaflet diffusional coupling by introducing a coupling parameter  $\lambda$  and comparing  $\lambda$  vs.  $c_{\text{tether}}$  for various polymer-tethered SOPC bilayers comprised of different lipopolymers, including dioctadecylamine [poly(2-ethyl-2-oxazoline) 4032] (DODA-E<sub>35</sub>,  $n = 35$ ) and 1,2-*O*-dioctadecyl-*sn*-glycero-3-[poly(2-methyl-2-oxazoline)]<sub>*n*</sub> (diC<sub>18</sub>-M<sub>15</sub>,  $n = 15$  and diC<sub>18</sub>-M<sub>50</sub>,  $n = 50$ ), and for a solid-supported SOPC bilayer ( $c_{\text{tether}} = 0$ ). Here  $\lambda$  is defined as the ratio of  $\langle r^2(c_{\text{tether}}) \rangle_{\text{inner}}$  to  $\langle r^2(c_{\text{tether}}) \rangle_{\text{outer}}$ . Based on this definition of  $\lambda(c_{\text{tether}})$ , which is given in eqn 4, maximum coupling occurs at  $\lambda(c_{\text{tether}}) = 1$ , whereas weaker coupling results in smaller values in the range of  $0 < \lambda(c_{\text{tether}}) < 1$ . The different lipopolymers were selected to obtain insight into the effect of polymer molecular weight on  $\lambda$  for a given  $c_{\text{tether}}$ . Fig. 4 illustrates the obtained  $\lambda$  vs.  $c_{\text{tether}}$  plots for polymer-tethered bilayers comprising DODA-E<sub>*n*</sub> (left) and diC<sub>18</sub>-M<sub>*n*</sub> (right). Fig. 4 (left) exhibits an offset between  $\lambda$  data of both DODA-E<sub>*n*</sub> ( $n = 35, 85$ ) systems with average values being  $\langle \lambda(c_{\text{tether}}) \rangle_{\text{DODA-E}_{85}} = 0.95$  and  $\langle \lambda(c_{\text{tether}}) \rangle_{\text{DODA-E}_{35}} = 0.69$ , respectively. A comparable offset can be found for membranes containing diC<sub>18</sub>-M<sub>*n*</sub> ( $n = 15, 50$ ) with  $\langle r^2 \rangle_{\text{diC}_{18}\text{-M}_{50}} = 0.95$  and  $\langle r^2 \rangle_{\text{diC}_{18}\text{-M}_{15}} = 0.6$  (Fig. 4, right). Importantly, the data in Fig. 4 show that the observed coupling of obstructed diffusion depends on the polymer molecular weight and that  $\lambda$  is largely independent of  $c_{\text{tether}}$ , at least, over a large range of  $0 \leq c_{\text{tether}} \leq 20$  mol%. Furthermore, the coupling parameters determined for the shorter chain systems, DODA-E<sub>35</sub> and diC<sub>18</sub>-M<sub>15</sub>, are very similar to that obtained for a solid-supported SOPC bilayer without lipopolymers, which was found to be  $\langle \lambda \rangle_{c_{\text{tether}} = 0} = 0.69$ . This similarity is not surprising because the bilayer–substrate distance of these particular bilayer systems is comparable, as verified on equivalent membrane systems using fluorescence

$\S$  The photolability of the fluorescent dye prevents long-term tracking of individual probe molecules, which is required for a more accurate determination of the diffusion type using  $\langle r^2 \rangle$ -time analysis to determine the type of diffusion.

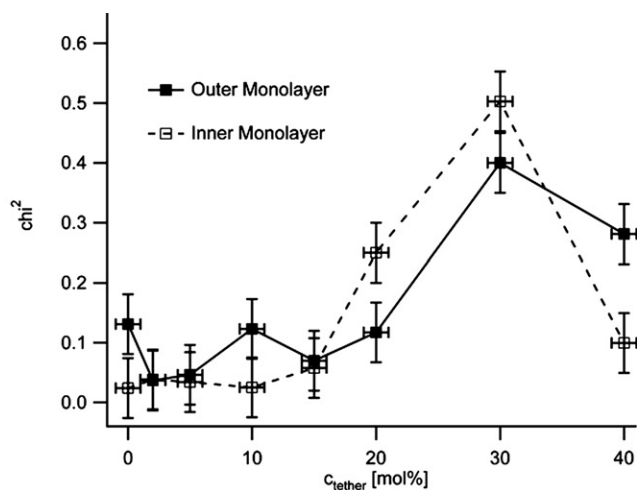
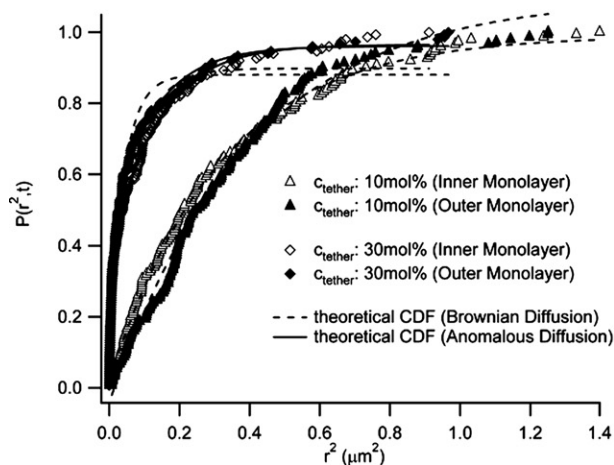


**Fig. 3** Representative experimental CDFs of the polymer-tethered bilayer based on DODA-E<sub>85</sub> at  $c_{\text{tether}} = 10, 30$  mol% and the corresponding theoretical CDFs using the Brownian (dashed) and anomalous (solid) diffusion models (left). Corresponding  $\chi^2$ - $c_{\text{tether}}$  plots of both monolayers of polymer-tethered membranes based on DODA-E<sub>35</sub> and DODA-E<sub>85</sub>, respectively, obtained from fitting analysis of experimental CDFs using the Brownian model (right).

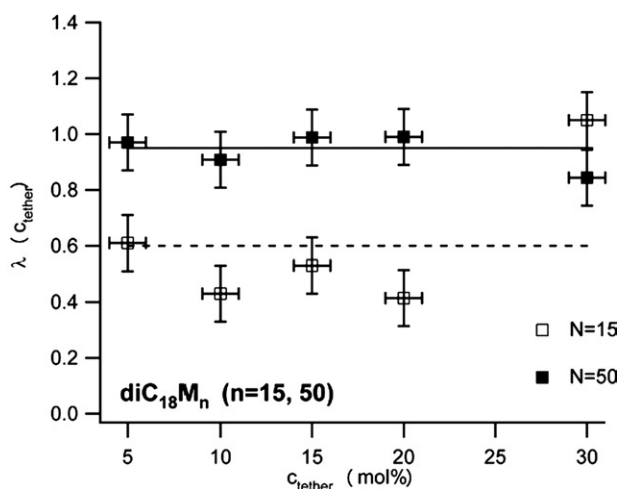
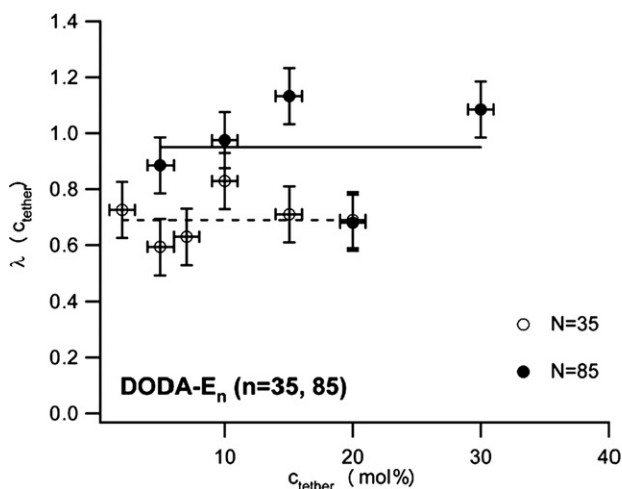


**Fig. 4**  $\langle \lambda \rangle$ - $c_{\text{tether}}$  plots of TRITC-DHPE in the inner and outer monolayers of the polymer-tethered bilayers consisting of DODA-E<sub>35</sub> and DODA-E<sub>85</sub> (left), as well as diC<sub>18</sub>-M<sub>15</sub> and diC<sub>18</sub>-M<sub>50</sub> (right). The data show strong coupling of obstructed diffusion for DODA-E<sub>85</sub> and diC<sub>18</sub>-M<sub>50</sub>, not observed for both shorter chain lipopolymer systems (DODA-E<sub>35</sub> and DODA-E<sub>85</sub>).

interference microscopy.<sup>30</sup> The notably higher  $\lambda$ -values observed for the polymer-tethered membranes containing higher molecular weight lipopolymers (DODA-E<sub>35</sub> and diC<sub>18</sub>-M<sub>50</sub>) are, however, remarkable. At low  $c_{\text{tether}}$ , one could simply argue that the stronger coupling is due to the enhanced bilayer-substrate distance, thus lowering asymmetric frictional coupling within the bilayer. At medium to high  $c_{\text{tether}}$ , however, where lipid diffusion is obstructed, the stronger coupling indicates an alternative mechanism: a polymer-induced inter-leaflet coupling of obstructed lipid diffusion. In the following, we discuss two potential explanations for such a mechanism.

One explanation assumes that the significant size mismatch between polymer and lipid moieties of lipopolymers and the interaction of phospholipids with polymer chains of lipopolymers in the vicinity of tethered lipids could lead to reduced packing densities around tethered lipids, causing localized acyl

chain interdigitation. To address this topic, we have conducted a set of control experiments by modifying the geometry of the tethered lipids from small dioctadecylamine (DODA)-anchors occupying an area per molecule of  $\sim 45\text{--}50 \text{ \AA}^2$  of DODA-E<sub>85</sub> to more spacious monounsaturated phospholipids 1,2-dioleoyl-*sn*-glycero-3-phosphoethanolamine (DOPE) occupying  $\sim 65 \text{ \AA}^2$  of 1,2-dioleoyl-*sn*-glycero-3-phosphoethanolamine-*N*-[methoxy (polyethylene glycol)-5000] (DOPE-PEG5000) lipopolymers. In the latter case, the lipid anchor is covalently linked to a poly(ethylene glycol) (PEG) chain of 110 monomer units. However, as illustrated in Fig. 5, tracking data obtained from polymer-tethered bilayers based on 5 and 30 mol% DOPE-PEG5000 again show comparable lipid diffusion in both bilayer leaflets, thus indicating strong coupling of obstructed lipid diffusion. Furthermore, previously it was reported that the degree of acyl chain interdigitation, as found in bilayers

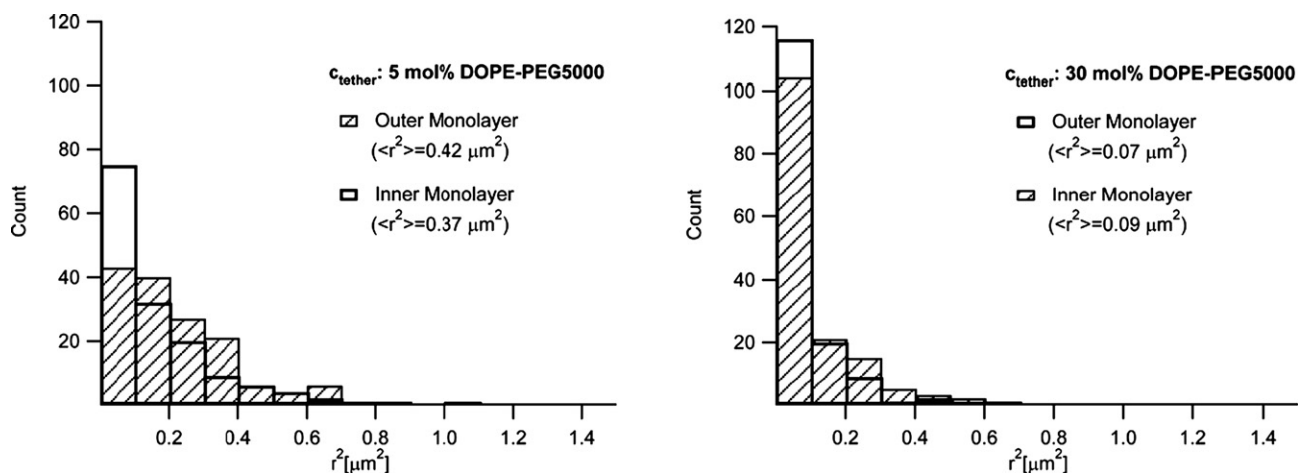


**Fig. 5** Comparison of  $r^2$  histograms and  $\langle r^2 \rangle$ -values obtained from TRITC-DHPE tracking experiments in the inner and outer monolayers of a polymer-tethered phospholipid bilayer consisting of DOPE-PEG5000 lipopolymer-tethers illustrated at  $c_{\text{tether}} = 5$  (left) and 30 mol% (right), respectively.

containing lipids of two different acyl chain lengths, does not affect the translational diffusion of lipids.<sup>26</sup> Consequently, different degrees of acyl chain interdigitation due to packing defects around tethered lipids are unlikely to alter the lipid diffusion and to explain the observed coupling of obstructed diffusion in polymer-tethered bilayers.

Another explanation is based on a mechanism in which coupling of obstructed diffusion in the polymer-tethered membrane is caused by deviations of the bilayer from the planar geometry, thus creating regions of high membrane tension. There is ample experimental evidence that membrane-anchored polymers induce shape changes in lipid vesicles.<sup>31,32</sup> Furthermore, it is well known that bending deformations of a membrane can cause tension, and that membrane strain is governed by the area compression modulus,  $K_A$ .<sup>33</sup> Previously, membrane bending phenomena have been studied theoretically by considering membranes bent around localized pinning points where membrane fluctuations are highly confined.<sup>34–39</sup> Interestingly, Nicolas and Safran have shown that there is a non-zero shear viscosity out of the plane of the bilayer around pinning points.<sup>38</sup> These authors argue that the resulting energy cost for the lateral movement of lipids can be rationalized by the fact that hydrophobic tails and hydrophilic heads of phospholipids interact among each other in the cone region, thus effectively leading to an increase in energy. We hypothesize that lipopolymers may form such pinning sites in polymer-tethered membranes and that the energy increase around each pinning point will affect both leaflets of the bilayer due to a significant morphological coupling between both leaflets of the bilayer, thus also obstructing their diffusion properties in a similar way, as shown in Fig. 1–4. Based on these findings, three types of bilayer deformations appear to be possible, which are schematically illustrated in Fig. 6: (A) lipopolymer-induced bilayer bending, (B) lipopolymer-induced membrane protrusions, and (C) partial self organization of lipopolymers into curved geometries. It would be beyond the scope of the current study to single out one of the three types of polymer-induced bilayer deformation. Nevertheless, in the following, these types will be discussed separately and experiments are presented to test the overall concept whether coupling

of obstructed diffusion can be caused by one or more of these polymer-induced bilayer deformations.

The first type of lipopolymer-induced bilayer deformation occurs in the absence of significant inter-polymer interactions at

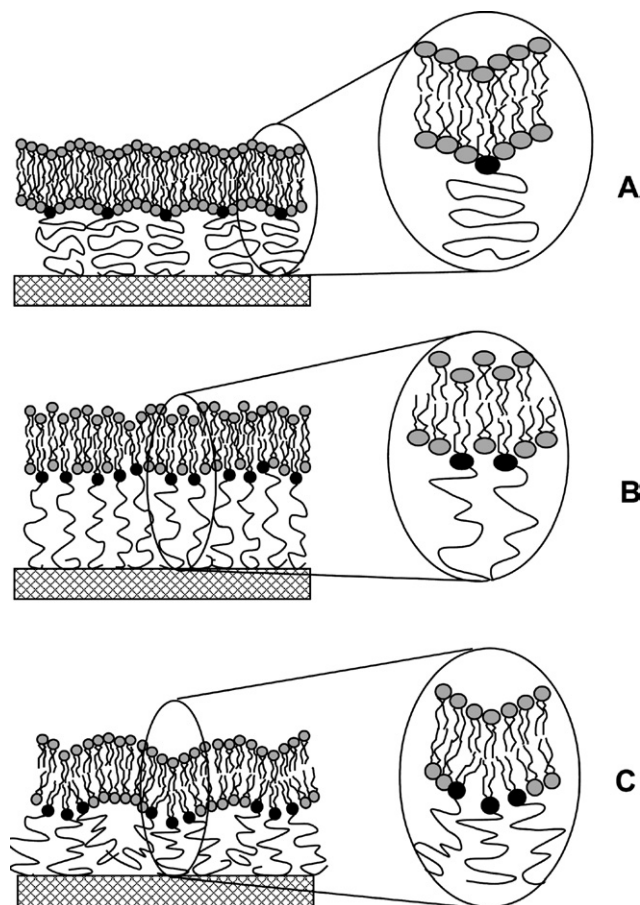


**Fig. 6** Schematic of possible lipopolymer-induced bilayer deformations in polymer-tethered membranes: (A) lipopolymer-induced bilayer bending; (B) lipopolymer-induced membrane protrusion; and (C) partial phase separation and self organization of lipopolymers.

low  $c_{\text{tether}}$ . It has been predicted theoretically that membrane-anchored polymers, such as those found in lipopolymers, may exert an entropic force due to the forced stretching of end-tethered polymer chains that this force causes the soft, elastic bilayer to bend away from the polymer.<sup>29,39</sup> In the case of low tethering concentrations (polymer mushrooms), the entropic force exerted by polymer chains is counterbalanced by the membrane bending elasticity (Fig. 6A). Because a polymer-tethered lipid represents a point defect in the membrane, sharp, cone-like bends can form.<sup>39</sup> At low tethering concentrations (polymer mushrooms), the spontaneous bending angle  $\psi$  of such cone-like bends can be expressed by:

$$\psi \approx T/2\pi\kappa \quad (1)$$

where  $T$  is the temperature and  $\kappa$  is the bending elasticity of the membrane.<sup>39</sup> Because no obstruction of lipid diffusion was observed at  $c_{\text{tether}} \leq 5$  mol% (Fig. 2), we do not expect that the above model is significant for the current study.

The second type of lipopolymer-induced bilayer deformation takes place in the presence of significant inter-polymer interactions among evenly distributed lipopolymers at elevated  $c_{\text{tether}}$ . At such elevated tethering concentrations (polymer brush), end-tethered polymers show an additional loss of entropy due to their confinement by neighboring polymers. In this case,  $\psi$  of a cone-like bend can be written as  $\psi \approx (T/\kappa)(R_p/s)^{2\nu}$  with  $R_p$  being the linear size of the tethered polymer,  $s$  being the average distance between tethering points, and  $\nu$  being a scaling exponent.<sup>39</sup>  $R_p$  can be approximated by the end-to-end distance of the polymer in solution  $R_p \approx aN^\nu$ , where  $a$  represents the persistence length and  $N$  is the number of monomers. Therefore, the entropy-driven deformations are not only dependent on the molecular weight and the end-to-end distance of tethered polymer chains, but also on  $c_{\text{tether}}$ . At higher  $c_{\text{tether}}$ , the close vicinity between the tethering points is likely to result in a deviation of the bilayer from a planar geometry, which resembles that of a bilayer exhibiting pronounced protrusions (Fig. 6B). The concept of pronounced protrusions is consistent with findings from neutron reflectometry studies on lipopolymer–lipid mixtures at the air–water interface.<sup>40</sup> There, it was argued that the protrusions are caused by enhanced water solubility of lipopolymers relative to lipids and by inter-polymer interactions. In the case of inter-polymer interactions, it has been hypothesized that the unfavorable osmotic pressure within the polymeric layer can be reduced *via* the roughening of the soft lipid layer, which is interfacial-energy costly. Protrusions will be less pronounced if the polymer chains of lipopolymers are end-tethered to the solid substrate. The latter argument could explain why Tanaka and coworkers reported no notable obstructed diffusion and coupling of obstructed diffusion over a large lipopolymer concentration range of  $c_{\text{tether}} = 0$ –20 mol%, where polymer-tethered membranes were designed using poly(2-methyl-2-oxazoline) lipopolymer diC<sub>18</sub>-M<sub>15</sub> ( $n = 14$  to 104) equipped with a terminal silane coupling group.<sup>11</sup> In the current study, protrusions are more likely because polymers are physisorbed somewhere along the polymer chain. This assertion is supported by our finding that strong coupling of obstructed diffusion can also be observed when the inner leaflet only contains a low concentration of tethered lipids ( $c_{\text{tether}} = 5$  mol%) and the lipopolymer molar concentration of the outer, non-

physisorbed, one is varied over the range of 5 mol%  $\leq c_{\text{tether}} \leq 30$  mol%. Corresponding  $\langle r^2 \rangle - c_{\text{tether}}$  plots are provided in the ESI†.

The third type of lipopolymer-induced bilayer deformation arises under conditions of heterogeneous lipopolymer distribution at elevated  $c_{\text{tether}}$ . Because physisorption makes lateral rearrangements of lipopolymers more likely, the formation of localized regions of high membrane curvature may also be caused by partial phase separation and self organization of lipopolymers, as illustrated in Fig. 6C. Lipopolymers are amphiphiles of conic shape with the polymer moiety being more spacious than the lipid anchor. Cone-shaped molecules, unlike many phospholipids, tend to self organize into highly curved structures, such as micelles. In particular, at medium to high  $c_{\text{tether}}$ , lipopolymers may escape the lateral stress in a polymer-tethered membrane by partially phase separating from lipids, thus forming lipopolymer-rich regions of high membrane curvature. Importantly, as lipopolymers with longer polymer chains have a more pronounced cone shape than their shorter chain counterparts, they will experience a higher lateral stress, thereby enhancing the tendency for self aggregation and/or protrusion at a given  $c_{\text{tether}}$ .

To test the concept of coupling of obstructed diffusion due to polymer-induced bilayer deformations experimentally, we added different amounts of cholesterol (CHOL) to the polymer-tethered SOPC bilayer, thus regulating bilayer bending elasticity as one of the critical parameters affecting membrane bending phenomena.<sup>39</sup> The rationale behind these experiments is that an enhanced bending elasticity (higher CHOL molar concentration) should reduce the degree of coupling of obstructed diffusion *via* the flattening of the lipid bilayer if the proposed model is correct. Indeed, this result is shown in Fig. 7 (left), where  $\langle r^2 \rangle$  data of TRITC-DHPE tracers in the inner and outer leaflets of a polymer-tethered bilayer at  $c_{\text{tether}} = 30$  mol% are compared as a function of CHOL molar concentration. Clearly, higher membrane CHOL concentrations lead to a weakened coupling of obstructed diffusion. It should be emphasized that the constant  $\langle r^2 \rangle$  data for the inner leaflet in Fig. 7 (left) do not necessarily imply that CHOL has no flattening effect on this leaflet. This is because the incorporation of CHOL into a polymer-tethered bilayer will likely enhance the lipid packing density, thereby reducing membrane lateral mobility, as previously reported on solid-supported membranes.<sup>41</sup> Consequently, the constant  $\langle r^2 \rangle$  data for the inner leaflet in Fig. 7 (left) is more likely the result of competing contributions, diffusion reduction *via* enhanced lipid packing and diffusion increase due to flattening of the leaflet. Fig. 7 (right) provides additional insight because it shows that in the presence of 30 mol% CHOL, the coupling of obstructed diffusion decreases with increasing  $c_{\text{tether}}$ . This result is intriguing because it suggests that the CHOL-induced flattening is different between both leaflets of the polymer-tethered bilayer, with the inner (lipopolymer-containing) leaflet being more resistant to CHOL-induced membrane flattening. Therefore, we hypothesize that at high  $c_{\text{tether}}$ , where decoupling of obstructed diffusion is observed, both leaflets of the bilayer are morphologically decoupled with the outer leaflet being flatter than the inner one.

Overall, the experimental findings in Fig. 7 support a model of coupling of obstructed lipid diffusion due to polymer-induced bilayer deformations around pinning points. Our data suggest that coupling of obstructed diffusion is most likely caused by

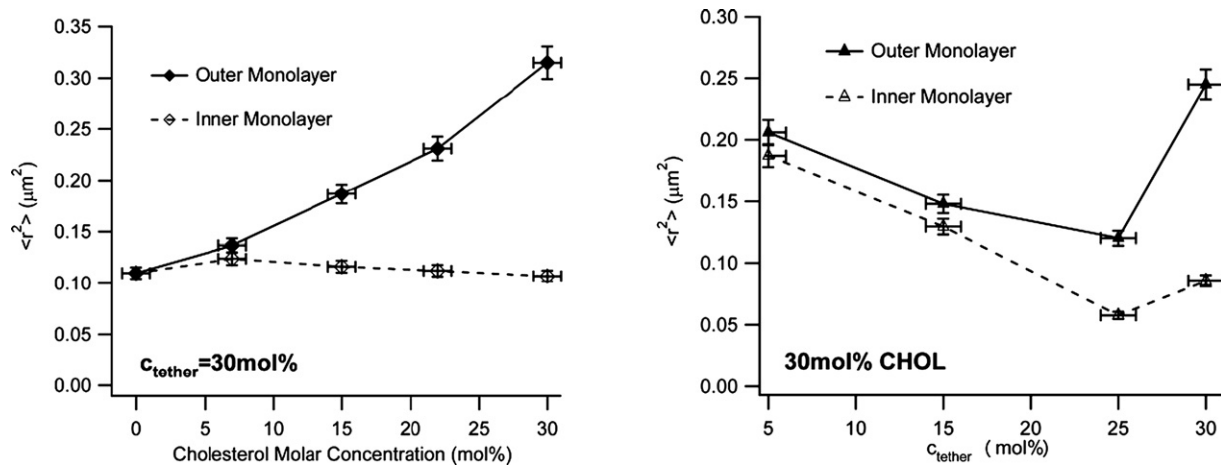


**Fig. 7** Role of CHOL on coupling of obstructed diffusion in polymer-tethered membranes containing DODA-E<sub>85</sub>:  $\langle r^2 \rangle$ -CHOL plots at constant  $c_{\text{tether}} = 30\text{ mol}\%$  (left) and  $\langle r^2 \rangle$ - $c_{\text{tether}}$  plots at 30 mol% CHOL (right). The graph shows enhanced decoupling of TRITC-DHPE lateral mobility with increasing CHOL content and  $c_{\text{tether}}$ , respectively.

lipopolymer-induced membrane protrusions and/or partial self organization of lipopolymers into curved geometries. We rationalize that analogous localized bilayer deformations may occur in biological membranes due to the interaction of bilayer constituents with the cytoskeleton and/or ECM, even though the control of membrane tension in cellular systems is quite complex. For example, it has been argued that the localized linkage of the cytoskeleton to the membrane causes stretching and deformation of the bilayer.<sup>42</sup> Our experimental results may provide a biophysical mechanism to explain the length-scale-dependent lateral diffusion of membrane proteins and phospholipids in plasma membranes if inter-compartmental diffusion barriers are based on non-membrane-spanning pickets such as lipid-based membrane attachments to the cytoskeleton. Our data may also be relevant to understand the ability of cone-shaped molecules in biomembranes (e.g., GPI-anchored proteins and glycolipids) to form membrane-spanning diffusion obstacles following their clustering into geometries of high membrane curvature. Finally, the experimental data obtained from CHOL-containing membranes shed light on an important interplay between obstructed diffusion, bilayer elasticity, and membrane composition. Obviously, there are still open questions. Most importantly, the structural properties of pinning points and the surface morphologies of both leaflets remain still unknown. Therefore, experiments are currently underway in our laboratory to explore the surface morphology and the possible formation of phase separations in polymer-tethered phospholipid bilayers in more detail. For example, such phase separations could also include the corralling of lipids by lipopolymers, as predicted theoretically and observed on poloxamer-lipid mixtures.<sup>43,44</sup>

## Experimental

### Materials

The lipopolymers dioctadecylamine [poly(2-ethyl-2-oxazoline) 8988] (DODA-E<sub>85</sub>) and dioctadecylamine [poly(2-ethyl-2-oxazoline) 4032] (DODA-E<sub>35</sub>) were synthesized following a procedure described recently.<sup>45</sup> The synthesis of 1,2-*O*-

dioctadecyl-*sn*-glycero-3-[poly(2-methyl-2-oxazoline)<sub>*n*</sub>] (*n* = 15 and 50) (diC<sub>18</sub>-M<sub>15</sub> and diC<sub>18</sub>-M<sub>50</sub>) was performed as described earlier.<sup>16,46-48</sup> The phospholipid, 1-stearoyl-2-oleoyl-*sn*-glycero-3-phosphocholine (SOPC) and the lipopolymer 1,2-dioleoyl-*sn*-glycero-3-phosphoethanolamine-*N*-[methoxy(polyethylene glycol)-5000] (DOPE-PEG5000) were purchased from Avanti Polar Lipids (Alabaster, AL). The fluorescently labeled phospholipid, *N*-(6-tetramethylrhodaminethiocarbonyl)-1,2-dihexadecanoyl-*sn*-glycero-3-phosphoethanolamine, triethylammonium salt (TRITC-DHPE) was obtained from Invitrogen/Molecular Probes (Eugene, OR). Chloroform (HPLC grade, Fisher Scientific, Pittsburgh, PA) was used as a spreading solvent for preparing SOPC and SOPC/lipopolymer monolayers at the air-water interface and Milli-Q water (pH = 5.5, 18 MΩ cm resistivity; Milli-Q, Millipore, Billerica, MA) was used as a subphase material for all experiments. The lipopolymer 1,2-dipalmitoyl-*sn*-glycero-3-phosphatidylethanolamine-*N*-[amino(polyethylene glycol) 2000]-TAMRA (DPPE-PEG2000-TAMRA) labeled with tetramethylrhodaminsuccinimidyl ester (TAMRA) was synthesized from the sodium salt of the amino functionalized lipopolymer (Avanti Polar Lipids, Alabaster, AL) and TAMRA (Invitrogen/Molecular Probes, Eugene, OR) according to our previously described procedure (yield: 70%, characterization by <sup>1</sup>H-NMR, FTIR spectroscopy and gel permeation chromatography).<sup>48</sup>

### Design of polymer-tethered phospholipid bilayer

As reported previously,<sup>13</sup> polymer-tethered phospholipid bilayers were built using successive Langmuir-Blodgett and Schaefer film transfers of SOPC/lipopolymer (lipopolymers employed: DODA-E<sub>85</sub>, DODA-E<sub>35</sub>, diC<sub>18</sub>-M<sub>15</sub>, diC<sub>18</sub>-M<sub>50</sub>, DOPE-PEG5000) and SOPC monolayers, respectively, between the air-water interface and substrate (glass cover slip of 24 × 40 mm<sup>2</sup> area) using a film balance with dipper (Labcon, Darlington, UK). Here the amphiphilic lipopolymers consisting of hydrophobic lipid and hydrophilic polymer moieties represent the crucial building block forming polymer-tethered lipids and allow for a straightforward adjustment of  $c_{\text{tether}}$ . The film pressure was adjusted at ~30 mN m<sup>-1</sup>, thus keeping the average area per lipid

affecting lipid lateral mobility constant at  $A_{\text{lipid}} = 65 \text{ \AA}^2$ . To allow for the monolayer-specific tracking of tracer molecules, small amounts ( $1 \times 10^{-8}$  mol%) of TRITC-DHPE were either added to the spreading solution of SOPC/lipopolymer before Langmuir–Blodgett transfer (tracking in inner monolayer) or to the spreading solution of SOPC before Schaefer transfer (tracking in outer monolayer).

### Single molecule fluorescence microscopy

Our wide-field single molecule fluorescence imaging setup was used as previously described.<sup>13</sup> A 200 mW frequency-doubled Nd:YAG laser (wavelength: 532 nm) was employed as an excitation source. The laser beam was spatially filtered and delivered to the EPI port of an inverted microscope (Zeiss Axiovert S100 TV, Zeiss, Oberkochen, Germany). Then the beam was reflected by a dichroic mirror (Omega XF1051, Omega Optical, Brattleboro, VT) and focused by a microscope objective (Zeiss, oil immersion,  $100\times$  NA = 1.3). The optical power was set so that the light intensity at the focus of the microscope objective was  $\sim 1.6 \text{ kW cm}^{-2}$ . To control photobleaching of the sample irradiated by the laser beam, a Uniblitz shutter (VMM-D1) of 3 mm open aperture was used. The fluorescence signal, centered at 566 nm, was passed through a  $2.5\times$  magnification lens and refocused to an intensified charge-coupled device camera (iPentaMAX 512EFT, Princeton Instruments, Roper Scientific, Trenton, NJ) mounted at the TV port of the microscope. The excitation light was blocked out by the combination of a Raman filter (Omega 540ELP) and the dichroic mirror. The temperature and the gain of the camera were set at  $-22 \text{ }^\circ\text{C}$  and 85.0, respectively. The exposure time and the frame rate of the charge-coupled device camera were chosen to be 10 ms and 16.7 frames  $\text{s}^{-1}$  while synchronized with the Uniblitz shutter using a time lag of  $t_{\text{lag}} = 50$  ms.

Image recording and single molecule tracking was conducted using *Isee* imaging software (Isee Imaging Systems, Raleigh, NC) running on a Linux platform. As described previously, tracking data were initially analyzed in terms of square displacements  $r^2$  at a constant time lag  $t_{\text{lag}} = 50$  ms.<sup>13</sup> To assure statistical significance, each sample was analyzed using 150 time steps of the same  $t_{\text{lag}} = 50$  ms (2–3 time steps were monitored per particle). This approach was chosen because photobleaching of the dye-label limits the number of position measurements per tracer molecule. In addition, one cannot measure longer time lags just by increasing the time interval between measurements because this risks losing the track due to on–off blinking of single dyes. The mean square displacement  $\langle r^2 \rangle$  values were calculated as described previously.<sup>13</sup> Based on the chosen number of time steps, an average  $r^2$  uncertainty per single histogram bar of  $\sim 10\%$  and a deviation in  $\langle r^2 \rangle$  of 1.5% can be obtained. These uncertainties were determined by repeating the tracking experiments on a newly prepared sample. By tracking the positional change of immobilized CdSe quantum dots, which are immobilized on glass, we determined the mechanical stability of the experimental setup and a lower limit for the displacement of mobile tracers which was found to be  $\sim 0.001 \text{ } \mu\text{m}^2$  ( $t_{\text{lag}} = 50$  ms). This value was used as a threshold to determine the immobile fraction,  $IF$ , from the tracking data determined.

To obtain information about the type of diffusion, the cumulative distribution function (CDF) was determined from the individual trajectories by counting the number of  $r^2$  with values  $\leq r^2$  and normalizing by the total number of tracks used. By using a time lag of  $t_{\text{lag}} = 50$  ms, the CDF method allowed us to probe a length scale of about 100 nm, which seems to be appropriate for the current study. Each CDF was analyzed assuming normal diffusion, for which the CDF is:<sup>49</sup>

$$P(r^2, t_{\text{lag}}) = 1 - \exp\left(-\frac{r^2(t_{\text{lag}})}{\langle r^2(t_{\text{lag}}) \rangle}\right) \quad (2)$$

, where  $\langle r^2(t_{\text{lag}}) \rangle$  is the mean square displacement and  $t_{\text{lag}} = 50$  ms. To analyze for anomalous subdiffusion, the tracking data were analyzed in terms of the theoretical CDF for anomalous diffusion:<sup>13</sup>

$$P(r^2, t) = \gamma(a, br^c)/\Gamma(a), \quad (3)$$

where  $\gamma(a, br^c)$  and  $\Gamma(a)$  are the incomplete and complete gamma functions, and  $a$ ,  $b$ , and  $c$  are constants. To describe the strength of diffusional coupling between both leaflets of the bilayer at a given  $c_{\text{tether}}$ , we defined a diffusional coupling parameter,  $\lambda(c_{\text{tether}})$ , with:

$$\lambda(c_{\text{tether}}) = \langle r^2 \rangle_{\text{inner}} / \langle r^2 \rangle_{\text{outer}} \quad (4)$$

Here  $\langle r^2 \rangle_{\text{inner}}$  and  $\langle r^2 \rangle_{\text{outer}}$  describe the experimentally determined  $\langle r^2 \rangle$  values from the inner and outer leaflets at a given  $c_{\text{tether}}$ .

### Acknowledgements

C. N. wants to thank M. Saxton, K. Jacobson, and R. Lipowsky for fruitful discussions. Funding was provided by the National Science Foundation (MCB-NSF 0416779). R. J. is thankful to the Deutsche Forschungsgemeinschaft for financial support through the Sonderforschungsbereich 563 “Bioorganic Functional Systems on Solids” (project A8-Jordan) and project JO287/4-1. Additional financial support by the Bavarian excellence network (CompInt) is also gratefully acknowledged.

### References

- 1 M. J. Saxton, *Curr. Top. Membr.*, 1999, **48**, 229–282.
- 2 A. Kusumi, C. Nakada, K. Ritchie, K. Murase, K. Suzuki, H. Murakoshi, R. S. Kasai, J. Kondo and T. Fujiwara, *Annu. Rev. Biophys. Biomol. Struct.*, 2005, **34**, 351–378.
- 3 T. Fujiwara, K. Ritchie, H. Murakoshi, K. Jacobsen and A. Kusumi, *J. Cell Biol.*, 2002, **157**, 1071–1082.
- 4 K. Murase, T. Fujiwara, Y. Umemura, K. Suzuki, R. Iino, H. Yamashita, M. Saito, H. Murakoshi, K. Ritchie and A. Kusumi, *Biophys. J.*, 2004, **86**, 4075–4093.
- 5 M. Tempel, W. H. Goldmann, C. Dietrich, V. Niggli, T. Weber, E. Sackmann and G. Isenberg, *Biochemistry*, 1994, **33**, 12565–12572.
- 6 W. Diakowski, A. Prychidny, M. Swistak, M. Nietubyc, K. Bialkowska, J. Szopa and A. F. Sikorsky, *Biochem. J.*, 1999, **338**, 83–90.
- 7 S. Mc Laughlin, J. Wang, A. Gambhir and D. Murray, *Annu. Rev. Biophys. Biomol. Struct.*, 2002, **31**, 151–175.
- 8 M. P. Sheetz, *Nat. Rev. Mol. Cell Biol.*, 2001, **2**, 392–396.
- 9 M. Wagner and L. K. Tamm, *Biophys. J.*, 2000, **79**, 1400–1414.
- 10 C. A. Naumann, O. Prucker, T. Lehmann, J. R uhe, W. Knoll and C. W. Frank, *Biomacromolecules*, 2002, **3**, 27–35.

- 11 O. Purrucker, A. Förtig, R. Jordan and M. Tanaka, *ChemPhysChem*, 2004, **5**, 327–335.
- 12 M. Wagner and L. K. Tamm, *Biophys. J.*, 2001, **81**, 266–275.
- 13 M. A. Deverall, E. Gindl, E.-K. Sinner, H. Besir, J. Rühle, M. J. Saxton and C. A. Naumann, *Biophys. J.*, 2005, **88**, 1875–1886.
- 14 R. Robolek, E. S. Lemker, B. Wiltschi, V. Kirste, R. Naumann, D. Oesterhelt and E.-K. Sinner, *Angew. Chem.*, 2007, **46**, 605–608.
- 15 O. Purrucker, S. Goennerwein, A. Foertig, R. Jordan, M. Rusp, M. Baermann, L. Moroder, E. Sackmann and M. Tanaka, *Soft Matter*, 2007, **3**, 333–336.
- 16 O. Purrucker, A. Förtig, K. Lüdtke, R. Jordan and M. Tanaka, *J. Am. Chem. Soc.*, 2005, **127**, 1258–1264.
- 17 O. Purrucker, A. Förtig, R. Jordan, E. Sackmann and M. Tanaka, *Phys. Rev. Lett.*, 2007, **98**, 078102.
- 18 L. Y. Hwang, H. Goetz, C. J. Hawker and C. W. Frank, *Colloids Surf., B*, 2007, **54**, 127–135.
- 19 L. Zhang and S. Granick, *Macromolecules*, 2007, **40**, 1366–1368.
- 20 L. Zhang and S. Granick, *Proc. Natl. Acad. Sci. U. S. A.*, 2005, **102**, 9118–9121.
- 21 R. Merkel, E. Sackmann and E. Evans, *J. Phys. F: Met. Phys.*, 1989, **50**, 1535.
- 22 L. Zhang and S. Granick, *J. Chem. Phys.*, 2005, **123**, 211104/1.
- 23 M. Hetzer, S. Heinz, S. Grage and T. M. Bayerl, *Langmuir*, 1998, **14**, 982.
- 24 S. E. Feller and R. W. Pastor, *J. Chem. Phys.*, 1999, **111**, 1281–1287.
- 25 A. Seelig and G. Seelig, *Biochemistry*, 1974, **13**, 4839–4845.
- 26 V. Schram and T. E. Thompson, *Biophys. J.*, 1995, **69**, 2517–2520.
- 27 J. M. Crane and L. K. Tamm, *Langmuir*, 2005, **21**, 1377–1388.
- 28 S. Garg, J. Rühle, K. Lüdtke, R. Jordan and C. A. Naumann, *Biophys. J.*, 2007, **92**, 1263–1270.
- 29 M. Breidenreich, R. R. Netz and R. Lipowsky, *Europhys. Lett.*, 2000, **49**, 431–437.
- 30 V. Kiessling and L. K. Tamm, *Biophys. J.*, 2003, **84**, 408–418.
- 31 J. Simon, M. Kühner, H. Ringsdorf and E. Sackmann, *Chem. Phys. Lipids*, 1995, **76**, 241–258.
- 32 V. Nikolov, R. Lipowsky and R. Dimova, *Biophys. J.*, 2007, **92**, 4356–4368.
- 33 D. Boal, 2002, *Mechanics of the Cell*, Cambridge University Press, Cambridge, UK, p. 151.
- 34 R. Bruinsma, M. Goulian and P. Pincus, *Biophys. J.*, 1994, **67**, 746–750.
- 35 D. Zuckerman and R. Bruinsma, *Phys. Rev. Lett.*, 1995, **74**, 3900–3903.
- 36 N. Gov, A. G. Zilman and S. Safran, *Phys. Rev. Lett.*, 2003, **90**, 228101/1.
- 37 N. Gov and S. Safran, *Phys. Rev. E*, 2004, **69**, 011101/1.
- 38 A. Nicolas and S. Safran, *Phys. Rev. E*, 2004, **69**, 051902.
- 39 R. Lipowsky, *Europhys. Lett.*, 1995, **30**, 197–202.
- 40 J. Majewski, T. L. Kuhl, M. C. Gerstenberg, J. N. Israelachvili and G. S. Smith, *J. Phys. Chem. B*, 1997, **101**, 3122–3129.
- 41 J. M. Crane and L. K. Tamm, *Biophys. J.*, 2004, **86**, 2965–2979.
- 42 K. Zeman, H. Engelhardt and E. Sackmann, *Eur. Biophys. J.*, 1990, **18**, 203–219.
- 43 G. Wu, J. Majewski, C. Ege, K. Kjaer, M. J. Weygand and K. Y. Lee, *Phys. Rev. Lett.*, 2004, **93**, 028101.
- 44 D. Zhang, M. A. Carignano and I. Szleifer, *Phys. Rev. Lett.*, 2006, **96**, 028701.
- 45 T. Lehmann, “Synthese von kovalent an Oberflächen fixierten Polyethyloxazolinfilmen zum Aufbau polymergestützter Biomembran-Modelle”, PhD dissertation, Universität Mainz, Mainz, Germany, 1999.
- 46 R. Jordan, K. Graf, H. Riegler and K. K. Unger, *Chem. Commun.*, 1996, **5**, 1025–1026.
- 47 R. Jordan, K. Martin, H. J. Räder and K. K. Unger, *Macromolecules*, 2001, **34**, 8858–8865.
- 48 T. Bonn , K. Lüdtke, R. Jordan, P. Štěpánek and C. M. Papadakis, *Colloid Polym. Sci.*, 2004, **282**, 833–843.
- 49 G. H. Schuetz, H. Schindler and T. Schmidt, *Biophys. J.*, 1997, **73**, 1073–1080.